Optimization and Engineering (2025) 26:199–227
https://doi.org/10.1007/s11081-024-09894-4

RESEARCH ARTICLE

Speed limits in traffic emission models using multi-objective optimization

Simone Göttlich[1] · **Michael Herty**[2] · **Alena Ulke**[1]

Received: 17 November 2023 / Revised: 17 May 2024 / Accepted: 28 May 2024 /
Published online: 18 June 2024

Abstract
Climate change compels a reduction of greenhouse gas emissions, yet vehicular traffic still contributes significantly to the emission of air pollutants. Hence, in this paper we focus on the optimization of traffic flow while simultaneously minimizing air pollution using speed limits as controllable parameters. We introduce a framework of traffic emission models to simulate the traffic dynamic as well as the production and spread of air pollutants. We formulate a multi-objective optimization problem for the optimization of multiple aspects of vehicular traffic. The results show that multi-objective optimization can be a valuable tool in traffic emission modeling as it allows to find optimal compromises between ecological and economic objectives.

Keywords Traffic flow network · Emission models · Multi-objective optimization · Numerical simulations

Mathematics Subject Classification 90B20 · 49K20 · 49M25 · 90B50

1 Introduction

The societal impact of vehicular traffic has increased significantly over the last years and so have its drawbacks affecting the public's health, the climate, and the environment (D'Amato and Cecchi 2008; Epstein 2005). As vehicular traffic emits air pollutants, it is directly linked to phenomena like air pollution, climate change, and global warming (Ramanatha and Feng 2009).

✉ Simone Göttlich
goettlich@uni-mannheim.de

Michael Herty
herty@igpm.rwth-aachen.de

Alena Ulke
ulke@uni-mannheim.de

[1] Department of Mathematics, University of Mannheim, 68131 Mannheim, Germany

[2] Department of Mathematics, RWTH Aachen University, 52056 Aachen, Germany

In this paper, we focus on the speed limit adjustments because (a) studies suggest that reducing speed limits reduces emissions (Int Panis et al. 2006), and (b) this countermeasure is easy and inexpensive to implement, while also having the added benefits of reducing traffic noise in urban areas, cf. Brink et al. (2022), and improving road safety, cf. Aljanahi et al. (1999).

The ubiquity of vehicular traffic has motivated a vast branch of research, namely the traffic flow modeling. The models developed range from micro- to macroscopic, and from first to second order, cf. Coclite et al. (2005), Garavello et al. (2016), Garavello and Piccoli (2006), Lighthill and Whitham (1955), Richards (1956), Treiber and Kesting (2013) for an overview. In particular, much attention has been paid to economic aspects of traffic such as travel time, ramp metering, or traffic flow and their optimization, e.g., by controlling speed limits or traffic lights, cf. Cascone et al. (2007), Goatin et al. (2016), Göttlich et al. (2015), Treiber and Kesting (2013). There is also a growing interest in modeling traffic emissions (Int Panis et al. 2006) and monitoring concentrations of air pollutants, e.g., by simulating their spread due to advection and diffusion (Stockie 2011). Recently, the idea of combining these approaches has been introduced in Alvarez-Vázquez et al. (2017), Balzotti et al. (2022), Berrone et al. (2012), Pasquier et al. (2023), Zegeye et al. (2011). Their common idea is to couple a traffic model with a model describing the dispersion of air pollutants. The coupling is achieved by estimating the emission of air pollutants based on quantities provided by the traffic flow model, and then, using this estimate as a source for the dispersion model. The authors of Alvarez-Vázquez et al. (2018) use this modeling approach to formulate an optimization problem aimed at finding the best extension of a road network to minimize traffic pollution. Furthermore, there is an increasing interest in jointly optimizing economic and environmental aspects of traffic. For example, Vázquez-Méndez et al. (2019) follows a cooperative approach. Here, the authors minimize traffic pollution while simultaneously minimizing travel times and maximizing the outflow of the network by controlling the network management, i.e., the incoming capacity of the roads and the drivers' preferences. The same problem is studied in García-Chan et al. (2022), where the authors instead follow a non-cooperative approach by formulating the problem as a bi-level Stackelberg game. The approach of joint optimization of economic and environmental aspects is also used in different applications such as wastewater management, cf. Alvarez-Vázquez et al. (2010, 2008), or the management of industrial plants (Alvarez-Vázquez et al. 2015).

We extend this line of research by addressing the following question: Is it possible to maximize an economic aspect of traffic, such as traffic flow, while also minimizing the contribution to air pollution by controlling speed limits? The novelty here lies in the approach to control the speed limits. We model this problem using multi-objective optimization.

First, we introduce the framework of speed-limit-dependent traffic emission models using a traffic, an emission, and a dispersion model where each depends on the quantities of the previous model. We illustrate this hierarchy in Fig. 1. The particular choice of these three models follows Alvarez-Vázquez et al. (2017) with an additional explicit speed limit dependence. Second, we formulate a multi-objective optimization problem aimed at maximizing traffic flow while simultaneously minimizing air pollution by controlling speed limits. Our approach to solve the proposed optimization uses

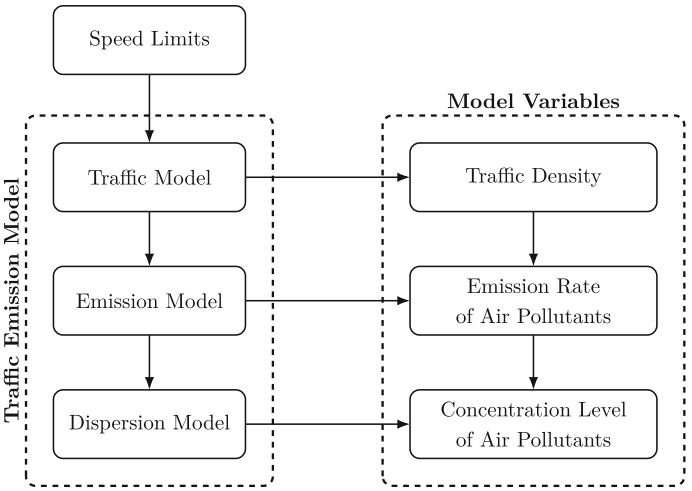

Fig. 1 Modeling framework of the traffic emission model including the dependence on the speed limits and the variables corresponding to the individual models

the *first-discretize-then-optimize* technique because the partial differential equations (PDEs) involved in the traffic emission model lack a closed-form solution in general.

This article is structured as follows: First, we introduce the framework of so-called speed-limit-dependent traffic emission models which is split into the traffic model (Sect. 2) and the emission and dispersion model (Sect. 3). Then, in Sect. 4, we derive a multi-objective optimization problem capturing the goal of maximizing traffic flow while minimizing air pollution. We cover the numerical treatment of our traffic emission model in Sect. 5 and conclude with a proof-of-concept example in Sect. 6.

2 Traffic flow dynamics

The traffic dynamic on a road network consists of two components: the traffic dynamics on the roads, and the coupling at the junctions. The traffic on the roads is described by a set of hyperbolic conservation laws, while the junctions are modeled by coupling conditions which encode boundary conditions at the end and beginning of each road (Coclite et al. 2005; Garavello et al. 2016; Garavello and Piccoli 2006).

A road network is a directed graph (V, E) where each edge $e \in E$ represents an unidirectional road associated with an interval $I_e = [0, L_e^{\text{road}}]$ and each vertex $v \in V$ represents a junction. A junction v can also be identified with a $(n+m)$–tuple $(e_1, \ldots, e_n, e_{n+1}, \ldots, e_{n+m})$ where the first n–tuple corresponds to the incoming and the second m–tuple to the outgoing roads of v, see also Coclite et al. (2005), Garavello et al. (2016), Garavello and Piccoli (2006). We call a junction an internal junction if it has roads directed both into and away from the node. Conversely, we refer to a junction as an external junction, if it has either roads directed into or away from the node.

2.1 The traffic dynamic on roads

We describe the traffic dynamic on the roads of a network according to the Lighthill–Whitham–Richards (LWR) model (Lighthill and Whitham 1955; Richards 1956), which characterizes it in terms of the traffic density $\rho_e(s,t)$ for given flux functions Q_e where $s \in I_e$ and $t \in \mathbb{R}^+$. For each road $e \in E$, the model reads

$$\partial_t \rho_e(s,t) + \partial_s Q_e(\rho_e(s,t), V_e^{\max}) = 0, \qquad \text{for } (s,t) \in I_e \times (0,T), \tag{2.1a}$$

$$\rho_e(s,0) = \rho_e^0(s), \qquad \text{for } s \in I_e. \tag{2.1b}$$

The flux functions Q_e are assumed to be dependent on the speed limits $V_e^{\max}$. The speed limits are constant over time and space, but may differ for every road. We set the flux function according to Greenshields' model (Greenshields et al. 1935):

$$Q_e(\rho, V_e^{\max}) := V_e^{\max} \rho \left(1 - \frac{\rho}{\rho_e^{\max}}\right),$$

where $V_e^{\max} > 0$ denotes the speed limit. The parameter $\rho_e^{\max}$ describes the maximal density. In the Greenshields model, the critical density $\rho_e^c := \arg\max_{0 \le \rho \le \rho_e^{\max}} Q_e(\rho, V_e^{\max})$ is independent of the speed limit policy as it is given by $\rho_e^c = \rho_e^{\max}/2$. The traffic densities are affected by the full speed limit policy due to the interaction of traffic at junctions. We denote the speed limit policy on the network by the vector $\boldsymbol{V}^{\max} = (V_e^{\max})_{e \in E}$ and hence, may write $\rho_e(s,t) = \rho_e(s,t,\boldsymbol{V}^{\max})$.

Notice, that the Greenshields' model is only one possible option. The following considerations can be carried out for strictly concave flux functions.

The model (2.1) is well-posed in the sense that it admits a (weak) solution for every road e if additional boundary conditions are given. The claim follows directly from Garavello et al. (2016), Garavello and Piccoli (2006) as for fixed speed limits $V_e^{\max}$, the model (2.1) coincides with the "classic" LWR model.

2.2 The traffic dynamic at junctions

To characterize the traffic at junctions, we impose suitable boundary conditions. In particular, we distinguish between two cases: boundary conditions stemming from an external junction, where we prescribe in- or outflow rates, and boundary conditions stemming from an internal junction, where the flow rates arise by coupling conditions, see e.g., Coclite et al. (2005), Garavello et al. (2016), Garavello and Piccoli (2006), Goatin et al. (2016).

At internal junctions, we suppose that the traffic dynamic obeys a physical condition, the conservation of mass. We follow Coclite et al. (2005), Garavello et al. (2016), Garavello and Piccoli (2006) and consider additional rules at a junction besides the conservation of mass:

(i) At an internal junction, the traffic distributes from the incoming to the outgoing roads according to fixed, time-independent parameters that encode the drivers' preferences.

(ii) At a merging junction, where the number of incoming roads is greater than the number of outgoing roads, fixed, time-independent parameters determine the priority among the incoming roads.
(iii) The drivers aim to maximize the flux across the junctions with respect to rule (i) or (ii), respectively.

These coupling conditions take the form of constrained maximization problems, one for each internal junction. Their solutions provide the in- and outflow at the boundary of the roads.

To express the coupling conditions explicitly, we define the demand and supply function for each road e:

$$D_e(\rho, V_e^{\max}) = \begin{cases} Q_e(\rho, V_e^{\max}), & \rho \le \rho_e^c, \\ Q_e^{\max}(V_e^{\max}), & \rho > \rho_e^c, \end{cases} \quad \text{and} \quad S_e(\rho, V_e^{\max}) = \begin{cases} Q_e^{\max}(V_e^{\max}), & \rho \le \rho_e^c, \\ Q_e(\rho, V_e^{\max}), & \rho > \rho_e^c. \end{cases}$$

and introduce the abbreviations:

$$\begin{aligned} D_i^{\text{in}}(t, \boldsymbol{V}^{\max}) &:= D_{e_i}(\rho_{e_i}(L_{e_i}^{\text{road}}, t, \boldsymbol{V}^{\max}), V_{e_i}^{\max}) && \text{for } i = 1, \dots, n, \\ S_j^{\text{out}}(t, \boldsymbol{V}^{\max}) &:= S_{e_j}(\rho_{e_j}(0, t, \boldsymbol{V}^{\max}), V_{e_j}^{\max}) && \text{for } j = n+1, \dots, n+m. \end{aligned}$$

Further, we introduce the following notation: The flow arriving at a junction from the incoming road e_i is denoted by $Q_{e_i}^{\text{in}}$. Similarly, we denote flow exiting the junction via the outgoing road e_j by $Q_{e_j}^{\text{out}}$. Then, the coupling condition at a junction at a fixed time $t \in [0, T]$ takes the form:

$$\max_{Q_{e_i}^{\text{in}}(t, \boldsymbol{V}^{\max})} \quad \sum_{i=1}^{n} Q_{e_i}^{\text{in}}(t, \boldsymbol{V}^{\max}) \tag{2.2a}$$

$$\text{subject to} \quad \underbrace{\sum_{i=1}^{n} \alpha_{j,i} Q_{e_i}^{\text{in}}(t, \boldsymbol{V}^{\max})}_{=: Q_{e_j}^{\text{out}}(t, \boldsymbol{V}^{\max})} \le S_j^{\text{out}}(t, \boldsymbol{V}^{\max}), \tag{2.2b}$$

$$0 \le Q_{e_i}^{\text{in}}(t, \boldsymbol{V}^{\max}) \le D_i^{\text{in}}(t, \boldsymbol{V}^{\max}), \tag{2.2c}$$

which is a linear optimization problem in finite dimensions. The parameters $\alpha_{j,i} \in (0, 1)$ encode the drivers' preferences among the incoming roads and have to satisfy: $\sum_{j=n+1}^{n+m} \alpha_{j,i} = 1$.

The maximization problem (2.2) admits a solution for fixed speed limits given some additional assumptions, see e.g., Garavello et al. (2016), making the distribution of traffic at a junction a well-posed problem. For an in-depth and rigorous discussion on coupling conditions at junctions, we refer to Garavello et al. (2016) and the references therein.

In the following, we provide the explicit solution to the maximization problem (2.2) for the case of the one-to-one, the diverging one-to-two, and the merging two-to-one junction since our proof-of-concept example in Sect. 6 is solely based on these three junctions. The solutions are taken from Goatin et al. (2016).

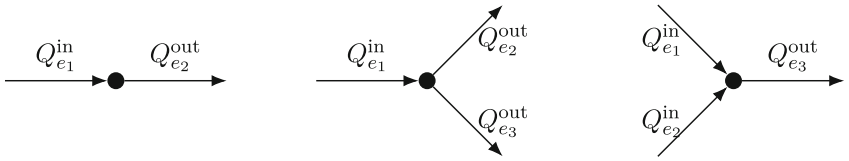

(a) One-to-one junction. (b) One-to-two junction. (c) Two-to-one junction.

Fig. 2 In- and out flow rates at the three basis junctions

We start with the one-to-one junction. In this case, the flux across the junction is given the minimum of the supply of the outgoing and the demand of the incoming road:

$$Q^{\text{in}}_{e_1}(t, \boldsymbol{V}^{\max}) = Q^{\text{out}}_{e_2}(t, \boldsymbol{V}^{\max}) = \min\{D^{\text{in}}_1(t, \boldsymbol{V}^{\max}), S^{\text{out}}_1(t, \boldsymbol{V}^{\max}))\}. \tag{2.3}$$

For the diverging one-to-two junction the parameter $\alpha_{j,i}$ describes the percentage of drivers arriving from road e_i at the junction, that take the outgoing road e_j. The fluxes across such a junction is given by

$$Q^{\text{out}}_{e_2}(t, \boldsymbol{V}^{\max}) = \min\{\alpha_{2,1} D^{\text{in}}_1(t, \boldsymbol{V}^{\max}), S^{\text{out}}_2(t, \boldsymbol{V}^{\max})\}, \tag{2.4a}$$

$$Q^{\text{out}}_{e_3}(t, \boldsymbol{V}^{\max}) = \min\{\alpha_{3,1} D^{\text{in}}_1(t, \boldsymbol{V}^{\max}), S^{\text{out}}_3(t, \boldsymbol{V}^{\max})\}, \tag{2.4b}$$

$$Q^{\text{in}}_{e_1}(t, \boldsymbol{V}^{\max}) = Q^{\text{out}}_{e_2}(t, \boldsymbol{V}^{\max}) + Q^{\text{out}}_{e_3}(t, \boldsymbol{V}^{\max}). \tag{2.4c}$$

The outflow of the incoming road is given by the sum of the inflow of the two outgoing roads, i.e., the number of vehicles entering the outgoing roads is the same as leaving the incoming road. Due to (2.4) the number of vehicles is preserved.

At a merging two-to-one junction the parameters $\beta_{j,i}$ regulate the priority of the incoming roads. The parameter $\beta_{3,i}$ describes the percentage of drives coming from the incoming road e_i that are allowed to take the only outgoing road:

$$Q^{\text{in}}_{e_1}(t, \boldsymbol{V}^{\max}) = \min\{D^{\text{in}}_1(t, \boldsymbol{V}^{\max}), \gamma_1\}, \tag{2.5a}$$

$$\text{where} \quad \gamma_1 := \max\{\beta_{3,1} S^{\text{out}}_1(t, \boldsymbol{V}^{\max}), S^{\text{out}}_1(t, \boldsymbol{V}^{\max}) - D^{\text{in}}_2(t, \boldsymbol{V}^{\max})\}, \tag{2.5b}$$

$$Q^{\text{in}}_{e_2}(t, \boldsymbol{V}^{\max}) = \min\{D^{\text{in}}_2(t, \boldsymbol{V}^{\max}), \gamma_2\}, \tag{2.5c}$$

$$\text{where} \quad \gamma_2 := \max\{\beta_{3,2} S^{\text{out}}_1(t, \boldsymbol{V}^{\max}), S^{\text{out}}_1(t, \boldsymbol{V}^{\max}) - D^{\text{in}}_1(t, \boldsymbol{V}^{\max})\}, \tag{2.5d}$$

$$Q^{\text{out}}_{e_3}(t, \boldsymbol{V}^{\max}) = Q^{\text{in}}_{e_1}(t, \boldsymbol{V}^{\max}) + Q^{\text{in}}_{e_2}(t, \boldsymbol{V}^{\max}). \tag{2.5e}$$

Next, we discuss the boundary conditions at external junctions. We distinguish between two cases: roads where vehicles exit the network, and roads where vehicles enter the network. In the first case, we assume free flow and in the second, we follow Goatin et al. (2016), Herty et al. (2009) and prescribe an inflow rate q^{in}_e and model a queue in case the desired inflow exceeds available capacity of the road. The queue can be interpreted as an infinitely long road with no spatial extension, and allows only feasible flow to be sent onto the network via the access roads. The modeling of a queue

can redistribute the inflow over time, allowing the flow to enter the network at a later point in time at which the capacity allows it. Further, we are interested in sending the maximal possible inflow. Thus, the evolution of the queue length ℓ_e obey the following ordinary differential equation (ODE):

$$\dot{\ell}_e(t) = q_e^{\text{in}}(t) - Q_e^{\text{out}}(t, \boldsymbol{V}^{\max}), \quad \ell_e(0) = \ell_e^0, \tag{2.6}$$

The flow rate Q_e^{out} describes the outflow from the queue onto the road and is therefore speed-limit-dependent. It is determined by the minimum between the capacity of the road, to ensure feasible flow rates, and the demand D_e^{queue} of the queue:

$$Q_e^{\text{out}}(t, \boldsymbol{V}^{\max}) = \min\left\{ D_e^{\text{queue}}(t), S_e(\rho_e(0, t, \boldsymbol{V}^{\max}), V_e^{\max}) \right\}. \tag{2.7}$$

The demand of the queue is composed of the prescribed inflow rate q_e^{in} and the flow rate q_e^{queue} that describes the flow required to clear the current queue connected to road e immediately, i.e.,

$$D_e^{\text{queue}}(t) = q_e^{\text{in}}(t) + q_e^{\text{queue}}(t). \tag{2.8}$$

The existence of a solution to the ODE (2.6) follows from Garavello et al. (2016) and the references therein. Again, we want to highlight that the evolution of the queue length depends on the fluxes on the roads, making it speed-limit-dependent and we may write $\ell_e(t) = \ell_e(t, \boldsymbol{V}^{\max})$.

3 Modeling air pollution caused by vehicular traffic

In this section, we cover the emission and dispersion model which simulate the traffic's contribution to air pollution. Our modeling approach is the following:

(i) The emission model estimates the emission rate of air pollutants on a given road based on the quantities the traffic model provides.
(ii) The dispersion model describes the spread of the pollutants in a two-dimensional domain Ω representing the simulated city. We include traffic's emission of pollutants by employing the estimate from (i).

3.1 The emission model

For the estimation of the emission rate, we follow Alvarez-Vázquez et al. (2018) and use a linear combination of the traffic density and traffic flow. Therefore, we introduce a weighting parameter $\theta \geq 0$ which represents the relative influence of the traffic density to the emission rate compared to the traffic flow. Also considering the speed-

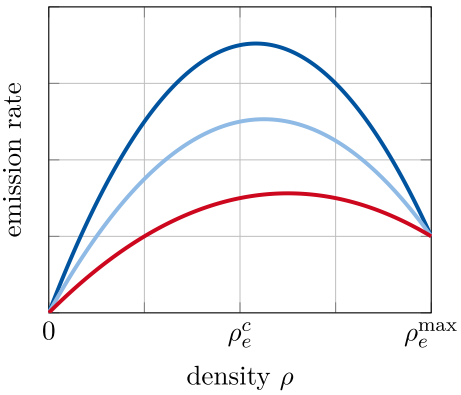

Fig. 3 Influence of the speed limit on the emission rate (3.1) for a fixed parameter $\theta > 0$. The corresponding speed limits are ordered as follows: $V_e^{\max}(red) < V_e^{\max}(lightblue) < V_e^{\max}(darkblue)$

limit dependence of the traffic density and flux function, the estimate of the emission rate ξ_e on road e reads:

$$\xi_e(s,t,\boldsymbol{V}^{\max}) = Q_e(\rho_e(s,t,\boldsymbol{V}^{\max}),\boldsymbol{V}^{\max}) + \theta\rho_e(s,t,\boldsymbol{V}^{\max}) \quad \text{for } (s,t) \in I_e \times (0,T). \tag{3.1}$$

For a fixed weighting parameter $\theta > 0$, we visualize the emission rate of road e in dependence on the traffic density in Fig. 3.

Furthermore, we assume that the road network represented by the graph (V, E), is contained in a domain $\Omega \subset \mathbb{R}^2$. To model the spread of air pollutants, which are emitted by vehicular traffic on the roads of a network, we introduce a source term that defines the emission rate at each point in Ω. Therefore, we parameterize each edge $e \in E$ by a curve $\sigma_e \colon I_e \to \Omega$. Its starting and end point are given by $\sigma_e(0)$ and $\sigma_e(L_e^{\text{road}})$, respectively to preserve the direction of e. See Fig. 4 for an illustration.

As the curves σ_e allow to identify a point $s \in I_e$ with a point $\boldsymbol{x} \in \Omega$, we map the values of the emission rates ξ_e to the two-dimensional domain Ω. Further, we assign a positive width w_e to each road and distribute the emission of air pollutants along the width w_e. Then the emission rate of road e within the domain Ω is:

$$\tilde{\xi}_e(\boldsymbol{x},t,\boldsymbol{V}^{\max}) = \begin{cases} \frac{1}{w_e}\xi_e(s,t,\boldsymbol{V}^{\max}), & \text{if } \boldsymbol{x} \in \mathcal{R}_e(s), \\ 0, & \text{otherwise,} \end{cases} \tag{3.2}$$

where the set $\mathcal{R}_e(s)$ describes the points along the width of the road e:

$$\mathcal{R}_e(s) := \left\{ \boldsymbol{x} \in \Omega \;\middle|\; \|\sigma_e(s) - \boldsymbol{x}\|_2 \le \frac{w_e}{2} \text{ and } \langle \sigma_e'(s), \sigma_e(s) - \boldsymbol{x} \rangle = 0 \right\}.$$

In Fig. 4b, we provide a visualization of this set for a road which is parallel to the y-axis. This example reveals one problem: Based on our modeling approach, for two roads $e \neq \tilde{e}$ the following relation can hold:

$$\mathcal{R}_e(s) \cap \mathcal{R}_{\tilde{e}}(\tilde{s}) \neq \emptyset \quad \text{where} \quad s \in I_e \text{ and } \tilde{s} \in I_{\tilde{e}}.$$

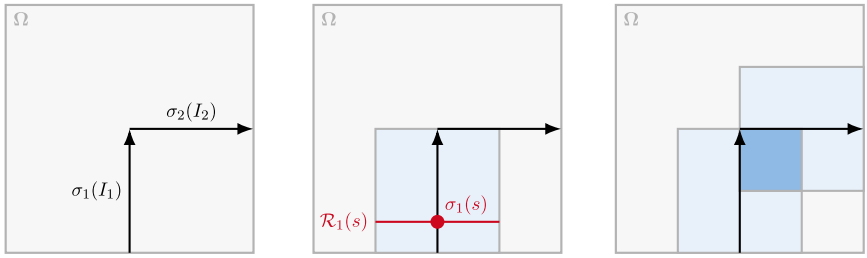

(a) Courses of the roads parameterized by the curves σ_1 and σ_2.

(b) Visualization of $\mathcal{R}_e(s)$ for road $e = 1$.

(c) Courses of the roads including the width $w_1 = w_2$.

Fig. 4 Points belonging to the grey shaded area are not associated to any road, while points belonging to the light blue shaded area are associated to a single road, and points belonging to dark blue shaded area are associated to two roads simultaneously. (color figure online)

This relation implies that there might exist points $\boldsymbol{x} \in \Omega$ to which multiple emission rates are assigned, see Fig. 4 for an illustration. This phenomenon also occurs when considering multiple, pairwise different roads, e.g., at junctions where more than two roads meet.

We resolve this problem by taking the average of the emission rates which are assigned to a point $\boldsymbol{x}$ based on the model given in Eq. (3.2). Therefore, we define the set $\mathcal{E}(\boldsymbol{x})$ that contains the roads to which the point $\boldsymbol{x}$ can be associated given $\{\sigma_e\}_{e\in E}$ and the width' $\{w_e\}_{e\in E}$ of the roads:

$$\mathcal{E}(\boldsymbol{x}) := \{e \in E \mid \boldsymbol{x} \in \boldsymbol{\mathcal{R}}_e\} \quad \text{with} \quad \boldsymbol{\mathcal{R}}_e := \bigcup_{s\in I_e} \mathcal{R}_e(s).$$

Thus, $|\mathcal{E}(\boldsymbol{x})|$ describes the number of roads assigned to $\boldsymbol{x}$. Finally, the joint emission rate defined on Ω, which is called *emission model* in the following, is given by:

$$\xi(\boldsymbol{x}, t, \boldsymbol{V}^{\max}) := \begin{cases} \frac{1}{|\mathcal{E}(\boldsymbol{x})|} \sum_{e\in\mathcal{E}(\boldsymbol{x})} \tilde{\xi}_e(\boldsymbol{x}, t, \boldsymbol{V}^{\max}), & \text{if } \mathcal{E}(\boldsymbol{x}) \neq \emptyset, \\ 0, & \text{otherwise.} \end{cases} \tag{3.3}$$

3.2 The dispersion model

After having established an estimate for the emission of air pollutants, we now introduce the dispersion model to simulate the spread of these pollutants within the domain Ω due to wind and horizontal diffusion. We follow the ideas of Alvarez-Vázquez et al. (2017), Balzotti et al. (2022), Parra-Guevara and Skiba (2003), Skiba and Parra-Guevara (2000), Stockie (2011) and invoke an advection–diffusion equation with suitable boundary conditions and make two assumptions: vehicular traffic is the only source of pollution in our model, i.e., pollutants cannot enter the domain from outside, but they can leave it due to wind and diffusion.

To formally represent these assumptions, we introduce the in- and outflow boundary of Ω for a given wind field. A wind field is a space- and time-dependent vector field $\mathbf{v} = (v_x, v_y)^\top$ and describes the wind dynamic in Ω. Additionally, we assume that Ω

is bounded, and its unit outward normal is denoted by $\vec{\eta}$. Then, the inflow boundary is defined by

$$S^-(\mathbf{v}) := \{(\boldsymbol{x}, t) \in \partial\Omega \times [0, T] \mid \mathbf{v}(\boldsymbol{x}, t) \cdot \vec{\eta}(\boldsymbol{x}) < 0\},$$

which describes the boundary through which pollutants enter the domain from outside due to the wind dynamic. Conversely, the outflow boundary describes the boundary where pollutants leave the domain due to the wind dynamic. Therefore, it is given by

$$S^+(\mathbf{v}) := \{(\boldsymbol{x}, t) \in \partial\Omega \times [0, T] \mid \mathbf{v}(\boldsymbol{x}, t) \cdot \vec{\eta}(\boldsymbol{x}) \geq 0\}.$$

Finally, given an initial concentration distribution ϕ_0 of the air pollutants in Ω, the following advection–diffusion equation describes the evolution of the concentration ϕ over time:

$$\partial_t \phi(\boldsymbol{x}, t) - \mu \Delta \phi(\boldsymbol{x}, t) + \mathbf{v} \cdot \nabla \phi(\boldsymbol{x}, t) + \kappa \phi(\boldsymbol{x}, t) = \xi(\boldsymbol{x}, t, \boldsymbol{V}^{\max}), \quad (\boldsymbol{x}, t) \in \Omega \times (0, T), \tag{3.4a}$$

$$\mu \nabla \phi(\boldsymbol{x}, t) \cdot \vec{\eta}(\boldsymbol{x}) - \phi(\boldsymbol{x}, t) \mathbf{v} \cdot \vec{\eta}(\boldsymbol{x}) = 0, \quad (\boldsymbol{x}, t) \in S^-(\mathbf{v}), \tag{3.4b}$$

$$\nabla \phi(\boldsymbol{x}, t) \cdot \vec{\eta}(\boldsymbol{x}) = 0, \quad (\boldsymbol{x}, t) \in S^+(\mathbf{v}), \tag{3.4c}$$

$$\phi(\boldsymbol{x}, 0) = \phi_0(\boldsymbol{x}), \quad \boldsymbol{x} \in \Omega, \tag{3.4d}$$

where the constant $\mu > 0$ describes the diffusion coefficient of the air pollutants and the constant κ their extinction rate to account for (chemical) interactions with other substances in the air. The boundary condition (3.4c) allows air pollutants to stream over the outflow boundary, whereas the boundary condition (3.4b) guarantees that the combined diffusive and advective flow is zero on the inflow boundary. The later condition enforces that pollutants cannot enter from outside.

The existence and uniqueness of a weak solution to the dispersion model (3.4) follows from Skiba and Parra-Guevara (2000, Theorem 1), which makes it a well-posed problem.

4 The multi-objective optimization approach

After introducing the traffic emission model in Sects. 2 and 3, our next goal is to maximize the economic efficiency of vehicular traffic while also minimizing the environmental impact by adjusting the speed limits on the roads. The formulation of the corresponding optimization problem is divided into two steps:

(i) The description of *economic efficiency* and the *environmental impact* by scalar-valued and speed-limit-dependent functions. Here, we use ideas already established in the literature.
(ii) The derivation of a multi-objective optimization problem where the functions obtained from (i) are optimized simultaneously. The approach of optimizing two aspects of traffic at the same time by controlling speed limits is unique in the traffic literature, at least to the best of our knowledge.

4.1 Quantification of economic and ecological aspects

The main concern of this section is the discussion on indicators in the form of scalar-valued, speed-limit-dependent functions to measure the economic and ecological aspects of vehicular traffic. The idea is to utilize the quantities provided by the traffic emission model, which include the traffic density and flux, or the concentration level of air pollutants.

The economic efficiency of vehicular traffic can be quantified by various aspects—for example, the travel time or the traffic flow, cf. Göttlich et al. (2015), Treiber and Kesting (2013). We maximize traffic flow by considering *accumulated traffic flow*:

$$\mathcal{J}_{\text{flow}}(\boldsymbol{V}^{\max}) := \sum_{e \in E} \int_0^T \int_{I_e} Q_e(\rho_e(s, t, \boldsymbol{V}^{\max}), V_e^{\max}) \, \mathrm{d}s \, \mathrm{d}t. \tag{4.1}$$

To determine the influence of vehicular traffic on the environment we measure its contribution to air pollution. Our modeling admits two sources: The *active* traffic on the road network and the *idle* traffic in the queues. The vehicles waiting in queues to enter the road network can contribute to air pollution since their engines may remain idle instead of being turned off. We measure the air pollution caused by the active traffic on the network by the average mass of air pollutant in a given control area Ω until a final time $T > 0$, cf. Alvarez-Vázquez et al. (2018):

$$\mathcal{J}_{\text{diff}}(\boldsymbol{V}^{\max}) := \frac{1}{T|\Omega|} \int_0^T \int_{\Omega} \phi(\boldsymbol{x}, t, \boldsymbol{V}^{\max}) \, \mathrm{d}\boldsymbol{x} \, \mathrm{d}t, \tag{4.2}$$

where $|\Omega|$ denotes the area of Ω. We measure the air pollution caused by idle traffic by the average amount of air pollutants emitted by idling vehicles waiting in queues. Assuming that all vehicles have the same emission rate when idle, we compute the pollution caused by idling vehicles based on the average queue length:

$$\mathcal{J}_{\text{queue}}(\boldsymbol{V}^{\max}) := \frac{1}{T} \sum_{e \in E_{\text{in}}} \int_0^T \ell_e(t, \boldsymbol{V}^{\max}) \, \mathrm{d}t, \tag{4.3}$$

where set E_{in} contains all access roads of the road network, i.e., roads at which we impose an external inflow rate q_e^{in}. Thus, an indicator for the influence of vehicular traffic on the environment based on air pollution is:

$$\mathcal{J}_{\text{poll}}(\boldsymbol{V}^{\max}; \delta) := \mathcal{J}_{\text{diff}}(\boldsymbol{V}^{\max}) + \delta \mathcal{J}_{\text{queue}}(\boldsymbol{V}^{\max}), \tag{4.4}$$

where $\delta \geq 0$ describes the emission of air pollutants per time unit of an idle engine.

Besides the expression 4.2 for $\mathcal{J}_{\text{diff}}$, we can employ another, equivalent one that allows us to solve a suitable PDE once, and then requires only a re-evaluation of the traffic model for each new speed limit policy, eliminating the need to solve the dispersion model. The derivation of the alternative expression is inspired by Alvarez-Vázquez et al. (2018) and involves integration by parts and some adjoint calculus. The

result reads:

$$\mathcal{J}_{\text{diff}}(\boldsymbol{V}^{\max}) = \int_0^T \int_\Omega \xi(\boldsymbol{x}, t, \boldsymbol{V}^{\max}) p(\boldsymbol{x}, t)\, \mathrm{d}\boldsymbol{x}\, \mathrm{d}t + \int_\Omega \phi_0(\boldsymbol{x}) p(\boldsymbol{x}, 0)\, \mathrm{d}\boldsymbol{x}, \quad (4.5)$$

where ϕ_0 is the initial data of the dispersion model (3.4), ξ is computed based on the emission model (3.3), and the adjoint p is the weak solution to the following adjoint equation:

$$-\partial_t p(\boldsymbol{x}, t) - \mu \Delta p(\boldsymbol{x}, t) - \mathbf{v} \cdot \nabla p(\boldsymbol{x}, t) + \kappa \tilde{p}(\boldsymbol{x}, t) = \frac{1}{T|\Omega|} \quad \text{for } (\boldsymbol{x}, t) \in \Omega \times (0, T), \quad (4.6a)$$

$$\mu \nabla p(\boldsymbol{x}, t) \cdot \vec{\eta}(\boldsymbol{x}) + \mathbf{v} \cdot \vec{\eta}(\boldsymbol{x})\, p(\boldsymbol{x}, t) = 0 \quad \text{for } (\boldsymbol{x}, t) \in S^+(\mathbf{v}), \quad (4.6b)$$

$$\nabla p(\boldsymbol{x}, t) \cdot \vec{\eta}(\boldsymbol{x}) = 0 \quad \text{for } (\boldsymbol{x}, t) \in S^-(\mathbf{v}), \quad (4.6c)$$

$$p(\boldsymbol{x}, T) = 0 \quad \text{for } \boldsymbol{x} \in \Omega. \quad (4.6d)$$

Again, the existence and uniqueness of a solution to the adjoint equation (4.6) follows from Skiba and Parra-Guevara (2000, Theorem 2), making the adjoint equation well-posed.

4.2 Multi-objective optimization involving traffic emission models

After having introduced functions to measure the economic efficiency and environmental impact of vehicular traffic, we now formulate an optimization problem that optimizes both aspects simultaneously. In other words, we try to optimize multiple objectives at the same time which leads us to the concept of multi-objective optimization.

The key components of a multi-objective optimization problem are the same as those of a classic, single-objective one: *Controls* $\boldsymbol{V} \in \mathbb{R}^d$, a *feasible set* $\mathcal{S} \subseteq \mathbb{R}^d$ encoding the constraints of the optimization if there are any, and $m \geq 2$ *objectives* $\mathcal{J}_i : \mathcal{S} \to \mathbb{R}$ to be minimized. The main difference to classical optimization is that we have multiple scalar-valued objectives $\mathcal{J}_i$ instead of a single one and we want to minimize all of them at once. The corresponding multi-objective optimization problem reads:

$$\min_{\boldsymbol{V} \in \mathcal{S}} \boldsymbol{\mathcal{J}}(\boldsymbol{V}) := (\mathcal{J}_1(\boldsymbol{V}), \ldots, \mathcal{J}_m(\boldsymbol{V}))\,. \quad (4.7)$$

The objectives $\mathcal{J}_i$ are typically conflicting which means that there exists no control $\tilde{\boldsymbol{V}}$ such that $\mathcal{J}_i(\tilde{\boldsymbol{V}}) = \min_{\boldsymbol{V} \in \mathcal{S}} \mathcal{J}_i(\boldsymbol{V})$ for all $i = 1, \ldots, m$. Hence, we characterize solutions to Eq. (4.7) with the help of Pareto optimality. For a comprehensive overview on multi-objective optimization and the concept of Pareto optimality see Branke et al. (2008), Ehrgott (2005) and the references therein.

A control $\boldsymbol{V}^*$ is called *Pareto optimal* if no component of $\mathcal{J}(\boldsymbol{V}^*)$ can be improved without deteriorating at least one of the others. The corresponding objective value $\mathcal{J}(\boldsymbol{V}^*)$ is called *efficient* and the set of all efficient points is called *Pareto front*. Thus, solving a multi-objective optimization problem correspond to the following task:

$$\min_{\boldsymbol{V}\in\mathcal{S}} \mathcal{J}(\boldsymbol{V}) \quad :\Leftrightarrow \quad \begin{cases} \text{Find all Pareto optimal controls } \boldsymbol{V} \in \mathcal{S}, \\ \text{and compute the Pareto front of } \mathcal{J}. \end{cases}$$

Now, we can formulate suitable multi-objective optimization problems that reflect our set goal of optimizing economic and environmental aspects of vehicular traffic at the same time by adjusting the speed limits on the roads. Our first ansatz is to measure economic efficiency by the accumulated traffic flow and the environmental impact by the average mass of air pollutant emitted by active and idle traffic. Altogether, this yields the following multi-objective optimization problem:

$$\min_{\boldsymbol{V}^{\max}\in\mathcal{S}} \left(-\mathcal{J}_{\text{flow}}(\boldsymbol{V}^{\max}),\ \mathcal{J}_{\text{poll}}(\boldsymbol{V}^{\max};\delta)\right) \tag{4.8a}$$

$$\text{where} \quad \mathcal{S} = \left\{ \boldsymbol{V}^{\max} \in (0,\infty)^d \mid \underline{V_e} \le V_e^{\max} \le \overline{V}_e \right\}. \tag{4.8b}$$

The scalar d denotes the number of roads within the road network. We also assume that the speed limit on each road is bounded from below and above by $\underline{V_e} > 0$ and $\overline{V}_e < \infty$, respectively to avoid $V_e^{\max} = 0$ and to mirror that traffic cannot be infinitely fast. Another ansatz is to minimize the environmental impact of active and idle traffic individually, i.e., splitting the objective $\mathcal{J}_{\text{poll}}$ into two, resulting in the multi-objective optimization problem:

$$\min_{\boldsymbol{V}^{\max}\in\mathcal{S}} \left(-\mathcal{J}_{\text{flow}}(\boldsymbol{V}^{\max}),\ \mathcal{J}_{\text{diff}}(\boldsymbol{V}^{\max}),\ \mathcal{J}_{\text{queue}}(\boldsymbol{V}^{\max})\right) \tag{4.9a}$$

$$\text{where} \quad \mathcal{S} = \left\{ \boldsymbol{V}^{\max} \in (0,\infty)^d \mid \underline{V_e} \le V_e^{\max} \le \overline{V}_e \right\},$$

with three objectives instead of two compared to the problem in (4.8).

The remainder of this paper focuses on solving the proposed multi-objective optimization problems, i.e., the computation of their Pareto fronts. We approach this in a *first-discretize-then-optimize* manner.

5 Numerical discretization

In this section, we derive discrete counterparts to our optimization problems (4.8) and (4.9). This requires the discretization of the traffic model (2.1), the emission model (3.3), and the adjoint equation (4.6) (as we invoke the expression (4.5) for $\mathcal{J}_{\text{diff}}$). With the discretization of the above, we can derive the discrete formulations for the objectives $\mathcal{J}_{\text{flow}}$, $\mathcal{J}_{\text{diff}}$, $\mathcal{J}_{\text{queue}}$, and $\mathcal{J}_{\text{poll}}$.

Because the emission model depends on the solution to the traffic model and the spatial domain of the adjoint equation, we cover its discretization after having intro-

duced the numerical treatment of the traffic model and the adjoint equation. Further, we omit the dependence on the speed limit policy $\boldsymbol{V}^{\max}$ in the following to improve the readability.

5.1 The traffic model

Before we discretize the traffic model with a finite volume scheme, cf. LeVeque (1992), we require a discretization of its temporal and spatial domain first. Therefore, we approximate the time horizon $[0, T]$ by an equidistant grid with N_t grid points and denote them by

$$t^k := k\Delta t \quad \text{with} \quad \Delta t := \frac{T}{N_t}, \tag{5.1}$$

where Δt is called *temporal step size*. For the discretization of the roads, we assume that all roads have the same length, i.e., the interval corresponding to the road e is given by $I_e = I$ where $I = [0, L^{\text{road}}]$. Then, we divide I into N_s cells I_n of equal length Δs which means

$$I_n := [s_{n-1}, s_n) \quad \text{where} \quad s_n = n\Delta s, \quad \text{and} \quad \Delta s = \frac{L^{\text{road}}}{N_s}. \tag{5.2}$$

Now, we can use a first-order finite volume scheme on each road to approximate the cell averages of the traffic densities on the cells I_n. For road e, we approximate the cell average of cell I_n at time t^k by $\rho_{e,n}^k$, i.e.,

$$\rho_{e,n}^k \approx \frac{1}{\Delta s} \int_{I_n} \rho_e(s, t^k)\, \mathrm{d}s.$$

Under the additional assumption that the real solution ρ_e is constant on each cell, we obtain the relation $\rho_e(s, t^k) \approx \rho_{e,n}^k$ if $s \in I_n$. Then, a finite volume scheme applied to the conservation laws of the traffic model (2.1) reads:

$$\rho_{e,1}^{k+1} = \rho_{e,1}^k - \frac{\Delta t}{\Delta s}\left[Q_e^{\text{num}}(\rho_{e,1}^k, \rho_{e,2}^k) - Q_e^{\text{out},k} \right], \tag{5.3a}$$

$$\rho_{e,n}^{k+1} = \rho_{e,n}^k - \frac{\Delta t}{\Delta s}\left[Q_e^{\text{num}}(\rho_{e,n}^k, \rho_{e,n+1}^k) - Q_e^{\text{num}}(\rho_{e,n-1}^k, \rho_{e,n}^k) \right] \text{ for } 1 < n < N_s, \tag{5.3b}$$

$$\rho_{e,N_s}^{k+1} = \rho_{e,N_s}^k - \frac{\Delta t}{\Delta s}\left[Q_e^{\text{in},k} - Q_e^{\text{num}}(\rho_{e,N_s-1}^k, \rho_{e,N_s}^k) \right], \tag{5.3c}$$

where Q_e^{num} is the so-called *numerical flux function* and estimates the flow between two neighboring cells based on their cell averages. We use the Godunov scheme where the corresponding flux function reads:

$$Q_e^{\text{num}}(u, v) = \min\{D_e(u), S_e(v)\}. \tag{5.4}$$

The quantities $Q_e^{\text{out},k}$ and $Q_e^{\text{in},k}$ describe the in- and outflow rates at the boundary of road e at time t^k, respectively and in the context of the traffic model are either given through external flow rates or internal coupling conditions. Notice, that we view the in- and outflow from the view of the connecting junctions, i.e., the outflow from the junction to an outgoing road e_j is equal to the inflow at the beginning of e_j and the inflow from an incoming road e_i to the junction is equal to the outflow at the end of e_i.

Remark 5.1 The temporal step size Δt of the numerical scheme (5.3) has to satisfy a CFL condition for every road e. For the numerical flux function (5.4) the CFL condition reads:

$$\frac{\Delta t}{\Delta s} a_e^{\max} \leq 1 \quad \text{where} \quad a_e^{\max} := \max \left\{ |Q_e'(\rho)| \;\middle|\; \min_{s \in I} \rho_e(s, t^k) \leq \rho \leq \max_{s \in I} \rho_e(s, t^k) \right\}. \tag{5.5}$$

Thus, we may need to take additional, intermediate time steps to advance from t^k to t^{k+1} where each step satisfies the CFL condition (5.5).

We provide a time-dependent inflow rate q_e^{in} for each access road e and model the corresponding queue by the ODE (2.6). To solve this ODE, we employ the explicit Euler scheme which results in the following equation:

$$\ell_e^{k+1} = \ell_e^k + \Delta t \left[q_e^{\text{in}}(t^k) - \min \left\{ q_e^{\text{in}}(t^k) + \frac{\ell_e^k}{\Delta t}, S_e(\rho_{e,1}^k) \right\} \right], \tag{5.6}$$

with initial condition $\ell_e^0 = 0$. To discretize the queue's demand D_e^{queue}, cf. Equation (2.8), we use $q_e^{\text{queue}}(t^k) \approx \ell_e^k / \Delta t$. The computation of the outflow of the queue $Q_e^{\text{out},k}$ to an access road then requires the evaluation of Eq. (2.7) while using the relations $\ell_e(t^k) \approx \ell_e^k$ and $\rho_e(0, t^k) \approx \rho_{e,1}^k$. In case e is an exit road, we obtain $Q_e^{\text{in},k}$ by recalling that we assume free flow at the end of the exist roads and utilizing the relation $\rho_e(L^{\text{road}}, t^k) \approx \rho_{e,N_s}^k$. Similarly, we compute the in- and outflow rates at internal junctions where we need to evaluate the Eqs. (2.3), (2.4) and (2.5).

5.2 The formal discrete adjoint equation

We require the solution to the adjoint equation (4.6) to evaluate $\mathcal{J}_{\text{diff}}$ according to Eq. (4.5). In order to utilize standard numerical methods for advection–diffusion-type equations, we transform $t \mapsto T - t$ to obtain the time-reversed adjoint equation which is formulated forward in time and which we solve by using finite differences.

We exemplify the numerical treatment by restricting the spatial domain to squares, i.e., for a fixed length L we have $\Omega = [0, L] \times [0, L]$ and by assuming that the diffusion coefficient μ and the wind field $\mathbf{v}$ are constant over time. This implies that the in- and outflow boundaries of Ω remain unchanged. Further, we denote the time-reversed adjoint by $\tilde{p}$.

First, we discretize the temporal and spatial domain, before delving into the numerical scheme in more detail. Since the spatial domain Ω is two-dimensional, we assume the number of grid points is the same in both directions. Therefore, we fix a number N_h of grid points and introduce the notation

$$x_i := ih, \quad y_j := jh \quad \text{with} \quad h := \frac{L}{N_h}, \tag{5.7}$$

where h is called *spatial step size*. This leads to the discrete and equidistant spatial domain Ω_h which is defined as follows

$$\Omega_h := \{(x_i, y_j) \mid 0 \leq i, j \leq N_h\}.$$

The temporal domain $[0, T]$ is discretized in the same fashion as for the traffic model, cf. Eq. (5.1).

5.2.1 Discretization of the time-reversed adjoint equation

The idea of finite differences is to approximate the solution of an PDE at the grid points. Hence, we introduce the notation $\tilde{p}(x_i, y_j, t^k) \approx \tilde{p}^k_{i,j}$ where $\tilde{p}^k_{i,j}$ is the numerical solution of the time-reversed adjoint equation which approximates the actual solution $\tilde{p}$. An approximation of the adjoint state p is then given through the relation:

$$p^k_{i,j} \approx p(x_i, y_j, t^k) = \tilde{p}(x_i, y_j, T - t^k) \approx \tilde{p}^{N_t - k}_{i,j}.$$

We discretize the time-reversed adjoint equation componentwise by approximating the temporal derivative with a forward difference:

$$\partial_t \tilde{p}(x_i, y_j, t^k) \approx \frac{1}{\Delta t}\left(\tilde{p}^{k+1}_{i,j} - \tilde{p}^k_{i,j}\right),$$

the Laplace operator $\mu \Delta \tilde{p}$ with the standard five-point stencil:

$$\mu \Delta \tilde{p}(x_i, y_j, t^k) \approx \Delta_{\text{diff}} \tilde{p}^k_{i,j} := \frac{\mu}{h^2}\left[\tilde{p}^k_{i,j+1} + \tilde{p}^k_{i,j-1} - 4\tilde{p}^k_{i,j} + \tilde{p}^k_{i+1,j} + \tilde{p}^k_{i-1,j}\right],$$

and the advection term $-\mathbf{v} \cdot \nabla \tilde{p}$, with the upwind scheme for both, the derivative with respect to x and with respect to y. We apply the scheme to $\tilde{\mathbf{v}} \cdot \tilde{p}$, where $\tilde{\mathbf{v}} = -\mathbf{v}$ to depict the correct direction of advection in the discrete equation, i.e.,

$$\tilde{\mathbf{v}} \cdot \nabla \tilde{p}(x_i, y_j, t^k) \approx \Delta_{\text{adv}} \tilde{p}^k_{i,j} := \frac{1}{h}\left[\tilde{v}_y^- \tilde{p}^k_{i,j+1} - \tilde{v}_y^+ \tilde{p}^k_{i,j-1} + \|\tilde{\mathbf{v}}\|_1 \tilde{p}^k_{i,j} + \tilde{v}_x^- \tilde{p}^k_{i+1,j} - \tilde{v}_x^+ \tilde{p}^k_{i-1,j}\right],$$

where for a scalar a, the identities $a^+ := \max\{a, 0\}$ and $a^- := \min\{a, 0\}$ hold. Altogether, by combining the discretization of these different components, we obtain an

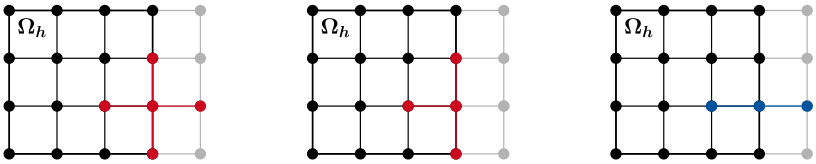

(a) A general five-point stencil. (b) A reduced five-point stencil. (c) The central-difference stencil.

Fig. 5 The black dots represent the grid, the red and blue dots a (reduced) five-point stencil and the stencil of a central difference respectively. The grey dots indicate the ghost points. (color figure online)

equation to compute the numerical solution for the next time step t^{k+1} provided the numerical solution at the current time step t^k is known:

$$\frac{1}{\Delta t}\left(\tilde{p}_{i,j}^{k+1} - \tilde{p}_{i,j}^{k}\right) - \Delta_{\text{diff}}\tilde{p}_{i,j}^{k} + \Delta_{\text{adv}}\tilde{p}_{i,j}^{k} + \kappa\,\tilde{p}_{i,j}^{k} = \frac{1}{T|\Omega|}. \tag{5.8}$$

Remark 5.2 Under the assumption that $\kappa = 0$, and that the wind field $\mathbf{v} = (v_x, v_y)^\top$ and the diffusion coefficient μ in (3.4) are constant over time, the CFL condition corresponding to the discretization (5.8) follows directly from (Wesseling 1996, Theorem 3.1 and Section 4) and reads:

$$\Delta t \le \frac{h^2}{4\mu + \|\mathbf{v}\|_1 h} \quad \text{and} \quad \Delta t\left[\frac{v_x^2}{2\mu + |v_x|h} + \frac{v_y^2}{2\mu + |v_y|h}\right] \le 1.$$

However, this CFL condition is invalid for $\kappa \neq 0$. Hence, we tighten the CFL condition to:

$$\Delta t \le \frac{1}{3}\frac{h^2}{4\mu + \|\mathbf{v}\|_1 h} \quad \text{and} \quad \Delta t\left[\frac{v_x^2}{2\mu + |v_x|h} + \frac{v_y^2}{2\mu + |v_y|h}\right] \le \frac{1}{3}. \tag{5.9}$$

We found that for our numerical experiments, the discretization (5.8) is stable given the tightened CFL condition (5.9). As this condition is independent of κ, one should not expect that it holds for all κ.

5.2.2 Discretization of the boundary conditions

The numerical scheme (5.8) suffers from a shortcoming: the stencils Δ_{diff} and Δ_{adv} applied to boundary values demand values of the numerical solution at inadmissible points, so-called *ghost points*, outside the domain Ω as illustrated in Fig. 5a. In the following, we provide a brief description of how to resolve this problem.

The (time-reversed) adjoint equation involves two types of boundary conditions: Neumann boundary conditions and Robin boundary conditions. Both determine the value of the solution implicitly through a differential equation.

The key idea to resolve the problem, is to utilize the ghost points when discretizing the Neumann and Robin boundary condition. We illustrate the method for the case

that the right boundary of Ω is a Robin boundary and discretize the corresponding Robin boundary condition as follows:

$$\mu \underbrace{\frac{\tilde{p}^k_{N_h+1,j} - \tilde{p}^k_{N_h-1,j}}{2h}}_{\approx \partial_x \tilde{p}(x_{N_h}, y_j, t^k)} + v_x \underbrace{\frac{\tilde{p}^k_{N_h+1,j} + \tilde{p}^k_{N_h-1,j}}{2}}_{\approx \tilde{p}(x_{N_h}, y_j, t^k)} = 0.$$

The corresponding stencil is visualized in Fig. 5c. Now, we can express the value $\tilde{p}^k_{N_h+1,j}$ at a ghost point by an admissible value of the numerical solution:

$$\tilde{p}^k_{N_h+1,j} = \frac{\mu - v_x h}{\mu + v_x h} \tilde{p}^k_{N_h-1,j}. \tag{5.10}$$

Finally, we can use the relation (5.10) to eliminate the inadmissable values from the stencils $\Delta_{\text{diff}} \tilde{p}^k_{N_h,j}$ and $\Delta_{\text{adv}} \tilde{p}^k_{N_h,j}$ which results in a reduced five-point stencil as illustrated in Fig. 5b. The approach in case the right boundary is a Neumann boundary is analogous and yields:

$$\tilde{p}^k_{N_h+1,j} = \tilde{p}^k_{N_h-1,j}.$$

5.3 The emission model

After having established the numerical treatment of the traffic model (2.1) and the adjoint equation (4.6), we proceed with approximating the emission rate ξ on Ω_h at given times t^k. Under the additional assumption that the traffic densities ρ_e are piecewise constant on the cells I_n, we approximate the emission rate of road e at time t^k by

$$\xi_e(s, t^k) \approx \tilde{\xi}^k_{e,n} := Q_e(\rho^k_{e,n}) + \theta \rho^k_{e,n} \quad \text{if} \quad s \in I_n.$$

Given these approximations, we invoke Equation (3.3), which directly yields an approximation of the emission rate ξ at a point $\boldsymbol{x} \in \Omega$ where $\mathcal{E}(\boldsymbol{x}) \neq \emptyset$ holds:

$$\xi(\boldsymbol{x}, t^k) \approx \xi^h(\boldsymbol{x}, t^k) := \frac{1}{|\mathcal{E}(\boldsymbol{x})|} \sum_{e \in \mathcal{E}(\boldsymbol{x})} \frac{1}{w_e} \tilde{\xi}^k_{e,n} \quad \text{if } \boldsymbol{x} \in R_e(s) \text{ and } s \in I_n.$$

Then, at a grid point (x_i, y_j) of the discrete control area, the approximation of the emission rate reads:

$$\xi(x_i, y_j, t^k) \approx \xi^k_{i,j} := \begin{cases} \xi^h(x_i, y_j, t^k), & \text{if } \mathcal{E}(x_i, y_j) \neq \emptyset, \\ 0, & \text{otherwise.} \end{cases} \tag{5.11}$$

Remark 5.3 The spatial step size of the advection–diffusion-type equation cannot be set arbitrarily. If, for example, the step size is too large, the road network is invisible

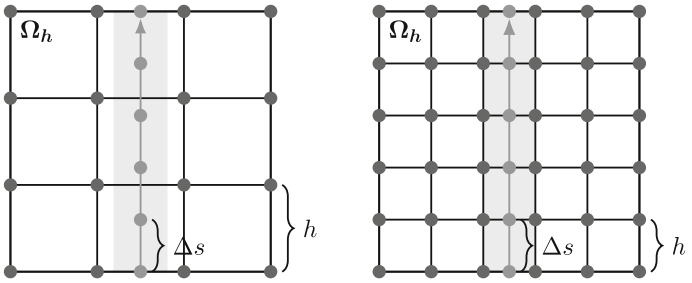

(a) Unsuitable spatial step sizes. (b) Suitable spatial step sizes.

Fig. 6 Illustration of suitable and unsuitable discretizations of Ω for a single-roaded network

to the discrete control area. We visualize the issue for a road network consisting of a single road in Fig. 6 including a discretization that is consistent with the length and width of the road as well as its positioning.

5.4 The objectives and the discrete optimization problem

Now given numerical solutions of the traffic model (2.1), the emission model (3.3), and the adjoint equation (4.6) with the schemes introduced above, we derive discrete versions of the objectives $\mathcal{J}_{\text{flow}}$, $\mathcal{J}_{\text{diff}}$, $\mathcal{J}_{\text{queue}}$, and $\mathcal{J}_{\text{poll}}$ based on the extended right rectangular rule for integrals.

Recall that the continuous variables depend on the speed limits, except for the adjoint state. Thus, the discrete variables inherit this dependence, which means we can write $\rho_{e,n}^k = \rho_{e,n}^k(\boldsymbol{V}^{\max})$, $\ell_e^k = \ell_e^k(\boldsymbol{V}^{\max})$, and $\xi_{i,j}^k = \xi_{i,j}^k(\boldsymbol{V}^{\max})$. This leads to the following discrete functions indicated by the superscript h:

$$\mathcal{J}_{\text{flow}}^h(\boldsymbol{V}^{\max}) = \Delta t h \sum_{e\in E}\sum_{k=1}^{N_t}\sum_{n=1}^{N_s} Q_e(\rho_{e,n}^k(\boldsymbol{V}^{\max}), \boldsymbol{V}^{\max}), \tag{5.12a}$$

$$\mathcal{J}_{\text{diff}}^h(\boldsymbol{V}^{\max}) = \Delta t h^2 \sum_{k=1}^{N_t}\sum_{i,j=1}^{N_h} \xi_{i,j}^k(\boldsymbol{V}^{\max}) p_{i,j}^k + h^2 \sum_{i,j=1}^{N_h} \phi_0(x_i, y_j) p_{i,j}^0 \tag{5.12b}$$

$$\mathcal{J}_{\text{queue}}^h(\boldsymbol{V}^{\max}) = \frac{\Delta t}{T} \sum_{e\in E_{\text{in}}}\sum_{k=1}^{N_t} \ell_e^k(\boldsymbol{V}^{\max}) \tag{5.12c}$$

$$\mathcal{J}_{\text{poll}}^h(\boldsymbol{V}^{\max}; \delta) = \mathcal{J}_{\text{diff}}^h(\boldsymbol{V}^{\max}) + \delta \mathcal{J}_{\text{queue}}^h(\boldsymbol{V}^{\max}). \tag{5.12d}$$

Given the discrete counterparts of the objectives, we can finally derive the discrete optimization problems by replacing the continuous objectives with the discrete ones. The optimization problem (4.8), where the goal is to maximize the traffic flow while

simultaneously minimizing the environmental impact, then becomes:

$$\min_{\boldsymbol{V}^{\max}\in\mathcal{S}} \left(-\mathcal{J}^h_{\text{flow}}(\boldsymbol{V}^{\max}), \mathcal{J}^h_{\text{poll}}(\boldsymbol{V}^{\max};\delta)\right), \tag{5.13}$$

while the optimization problem (4.9) which involves three objectives, becomes:

$$\min_{\boldsymbol{V}^{\max}\in\mathcal{S}} \left(-\mathcal{J}^h_{\text{flow}}(\boldsymbol{V}^{\max}), \mathcal{J}^h_{\text{diff}}(\boldsymbol{V}^{\max}), \mathcal{J}^h_{\text{queue}}(\boldsymbol{V}^{\max})\right). \tag{5.14}$$

The discrete optimization problems (5.13) and (5.14) can be solved by standard methods to solve multi-objective optimization problems as the discrete objectives allow a direct evaluation by invoking the numerical schemes introduced previously.

6 Numerical experiments

In this section, we aim to gain an insight into the trade-off between maximizing economic efficiency and minimizing the environmental impact. To achieve this, we solve the discretized multi-objective optimization problems (5.13) and (5.14) with fixed coefficients and step sizes, providing a proof-of-concept example. Furthermore, we study the impact of the presence of idle traffic on the solution of the optimization problem (4.8). We distinguish between two cases: when the function $\mathcal{J}_{\text{poll}}$, measuring air pollution, only considers the active traffic in the network ($\delta = 0$), and when it also takes the idle traffic in the queues into account ($\delta > 0$), cf. Eq. (5.12d). Additionally, we compare the results to the solution of the optimization problem (4.9) which minimizes the contribution of active and idle traffic to air pollution individually.

We solve the resulting multi-objective optimization problems using the `paretosearch` function from Matlab's *Optimization Toolbox* (MATLAB and Optimization Toolbox Release 2022). This function is based on pattern search on a set of points. It iteratively searches for efficient points that are close to the true Pareto front.

6.1 Definition of the proof-of-concept example

In this section, we present an overview of our model and discretization parameters (Table 1). The road network along with the initial data is shown in Figs. 7a, b and the spatial discretization of the traffic model is illustrated in Fig. 7c.

In the following, we also comment briefly on the choice of the essential parameters.

For the traffic model, we opt for the common academic parameters. This means all roads have a unit length of $L_e^{\text{road}} = 1$ and the same maximal capacity of $\rho_e^{\max} = 1$. For the initial density distribution, we assume that the initial densities are constant along each road. Motivated by the academic scenario where typical speed limits are $V_e^{\max} = 1$, we impose box constraints that bound the minimal and maximal allowed

Table 1 Overview of the parameter values defining the proof-of-concept example

Parameter	Value
Traffic model	
T	5
I_e	[0, 1]
$\rho_e^{\max}$	1
q_e^{in}	0.25
ρ_e^0	cf. Fig. 7b
σ_e	cf. Fig. 7a
$\alpha_{j,i}$,	0.5
$\beta_{j,i}$	0.5
Emission model	
Ω	$[0, 3] \times [0, 3]$
w_e	0.1
θ	0.5
Dispersion model	
$\mathbf{v}$	$(1, 1)^\top$
κ	0
μ	10^{-6}
ϕ_0	0
Optimization	
$\underline{V_e}$	0.25
$\overline{V_e}$	2
Discretization	
$\Delta s, h$	0.05
N_s	20
N_h	60
Δt	0.0083
N_t	601

speed limit on a road as follows:

$$\mathcal{S} = \left\{ \boldsymbol{V}^{\max} \in \mathbb{R}^6 \;\middle|\; \frac{1}{4} \leq V_e \leq 2 \text{ for all } e \in E \right\}.$$

Next, we suppose that in the dispersion model, the advection dominates the spread of air pollutants. This assumption is reasonable because for gases a diffusion coefficient of around $10^{-6}\text{m}^2\,\text{s}^{-1}$ is typical, which is significantly smaller than a wind velocity of around 1ms^{-1} that indicates calm air conditions.

Further, we assume that the control area Ω is initially free of air pollutants, which implies

$$\phi(\boldsymbol{x}, 0) = \phi_0(\boldsymbol{x}) = 0 \quad \text{for all} \quad \boldsymbol{x} \in \Omega.$$

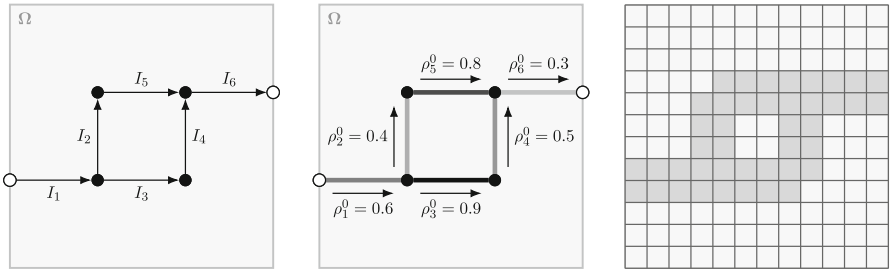

(a) Road network in Ω. (b) Initial data. (c) Schematic discretization.

Fig. 7 The road network of the proof-of-concept example. The schematic spatial discretization includes the width of the roads

Notice that this does not depict the real world. However, the alternative expression (4.5) of the objective $\mathcal{J}_{\text{diff}}$ reveals that the term involving ϕ_0 is independent of the speed-limits. In other words, the choice of ϕ_0 only results in a constant shift in $\mathcal{J}_{\text{diff}}$ and thus has no effect on the minimizers of $\mathcal{J}_{\text{diff}}$ and $\mathcal{J}_{\text{poll}}$. Therefore, this assumption is unrestrictive.

To close the discussion on parameter selection, it is worth noting that the temporal step size Δt and the spatial step size h have to satisfy a CFL condition for the time-reversed adjoint equation, cf. Remark 5.2, to ensures the stability of the numerical scheme.

After we have established the parameter choices, we analyze the solution of the optimization problem (4.8) for different values of δ next. Afterwards, we compare these optimal solutions to the one of (4.9).

6.2 Results of the numerical experiments

Before we continue with a detailed discussion of the results, let us comment on the choices of δ which are used to showcase and compare optimal solutions.

The parameter δ regulates the influence of idle traffic on the caused air pollution. The choice $\delta = 0$ represents the case where idle traffic has no effect on the environment, while for $\delta > 0$ idle traffic also contributes to air pollution, cf. Eq. (5.12d). Hence, we consider $\delta \in \{0, \frac{1}{2}\}$ to showcase the influence of idle traffic on air pollution and optimal speed limits.

We begin by solving the proof-of-concept example with $\delta = 0$. In this scenario the presence of a queue with idle vehicles has no impact on the environment.

In Fig. 8, we visualize the resulting optimal solution, including the Pareto front in Fig. 8a. Notice that the ideal vector and the Pareto front are located in the lower right corner of the plot instead of the lower left corner because we maximize $\mathcal{J}_{\text{flow}}^h$. Furthermore, the axes of Fig. 8a are normalized by the optimal values of the objectives, i.e., the accumulated traffic flow and the indicator to measure the caused air pollution are divided by

$$\max_{\boldsymbol{V}^{\max} \in \mathcal{S}} \mathcal{J}_{\text{flow}}^h(\boldsymbol{V}^{\max}) \quad \text{and} \quad \min_{\boldsymbol{V}^{\max} \in \mathcal{S}} \mathcal{J}_{\text{poll}}^h(\boldsymbol{V}^{\max}; \delta),$$

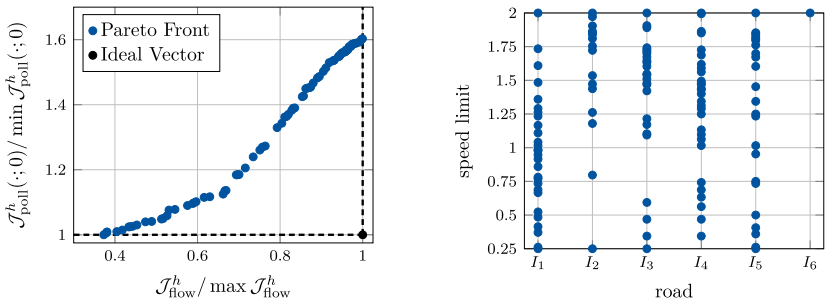

(a) Pareto front and ideal vector.

(b) Values of the Pareto-optimal speed limit policies.

Fig. 8 The optimal solution of the proof-of-concept example with $\delta = 0$, i.e., air pollution is sorely estimated by active traffic on the road network

respectively. Hence, the axes represent the relative difference of the function values compared to the optimal value, which is given by one as the ideal vector becomes $(1, 1)^\top$ for the normalized objectives.

For example, Fig. 8a shows that sorely minimizing the contribution to air pollution results in the efficient point $(0.37, 1)^\top$. This point translates to: while the contribution to air pollution is minimal, the accumulated traffic flow decreases by 63% compared to its ideal value. The reversed case yields the efficient point $(1, 1.6)^\top$ where we maximize the economic efficiency. Here the environmental impact increases by 60% compared to its ideal value while the accumulated traffic flow attains its maximum.

An example for an efficient point where neither of the objectives attains its optimum, is the point $(0.8, 1.34)^\top$. Here the environmental impact is increased by 34% while the economic efficiency decreases by 20%.

Because each efficient solution of the Pareto front corresponds to a Pareto-optimal speed limit policy, we investigate the Pareto-optimal speed limit policies in more detail now.

Figure 8b shows the computed Pareto-optimal speed limits of the individual roads. Notice this provides information on the range of the optimal speed limits of a road but not on the concrete optimal policies since those are vectors, i.e., randomly connecting the optimal speed limits of the individual roads illustrated in Fig. 8b, does not yield an optimal policy. Nevertheless, Fig. 8b reveals that the two objectives are conflicting as the range of the optimal speed limits nearly covers the entire interval [0.25, 2] for each road, except for the exit road $e = 6$. At the exit road, the two objectives "agree" on an optimal speed limit, i.e., $V_6^{\max} = 2$. A possible explanation may be that, as we impose free flow at the exit road and the initial density of this road is relatively low, the vehicles should and can leave the network as fast as possible because then they do not contribute to the air pollution anymore—at least from the modeling point of view. Further, the flux function scales linearly with the speed limit, i.e., for a fixed density, the traffic flow increases as the speed limit increases, resulting in a higher traffic flow.

On the other hand, we visualize certain speed limit policies along the two routes of the road network in Fig. 9 to gain an impression of what optimal speed limit policies look like and if they impose any difficulties considering real-world applications. The

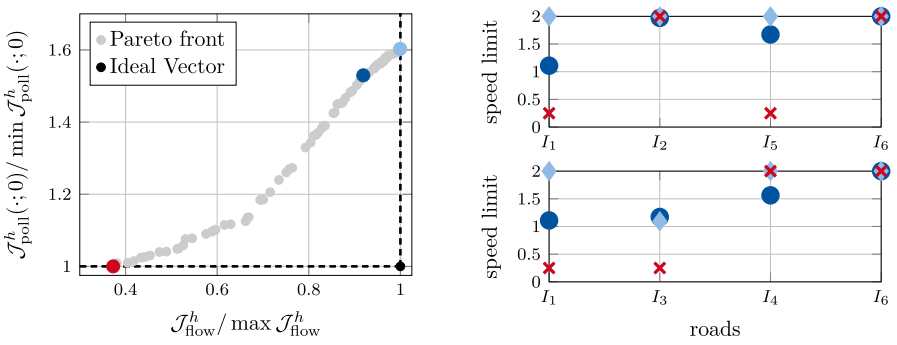

(a) Pareto front and ideal vector. (b) Speed limit policies along the routes.

Fig. 9 Pareto-optimal speed limit policies along the two routes of the sample road network. The correspondence between efficient solutions and the Pareto-optimal speed limit policies is color-coded (in red, dark blue and light blue)

two routes a driver can take are the "lower" and "upper" route, which are given by

$$I_1 \to I_3 \to I_4 \to I_6 \quad \text{and} \quad I_1 \to I_2 \to I_5 \to I_6,$$

respectively, see Fig. 7a.

The speed limits policy corresponding to the efficient solution, where $\mathcal{J}^h_{\text{poll}}$ attains its minimum, is a bang-bang control, i.e., the speed limits are either given by the lower or upper bound of the inequality constraint. Along the upper route, the speed limits alternate between the lower and upper bound. Even though this is unproblematic from the mathematical point of view, it may be in real-world applications because in reality, drivers may violate the lower speed limit when coming from a high-speed-limit road.

A similar problem occurs at the diverging junction, where the speed limits of the outgoing roads are $V_2^{\max} = 0.25$ and $V_3^{\max} = 2$. Again, this does not impose a mathematical problem, but in the real world, drivers can "choose" between the outgoing roads, and hence, a majority may opt for road $e = 3$ because it allows higher speeds. However, at each diverging junction, we prescribe speed-limit-independent distribution rates to describe the percentage of incoming drivers accessing an outgoing road. Hence, a higher speed limit creates an incentive to opt for the corresponding road, which then results in a violation of the modeled distribution rates, i.e., the model does not depict the reality anymore. Both issues present a subject of future research: adjusting the constraints on the speed limit policies to avoid a big difference between consecutive speed limits or speed limits of outgoing roads at a junction.

Another speed limit policy in Fig. 9 is marked in dark blue, where neither of the objectives attains its optimum. This speed limit policy shows a similar behavior compared to the one corresponding to minimal environmental impact, but the increase of the speed limits along the lower route is shallower. Further, the lowest speed limit along the upper route is around $V_e^{\max} \approx 0.6$ compared to $V_e^{\max} = 0.25$ for the example of minimal environmental impact.

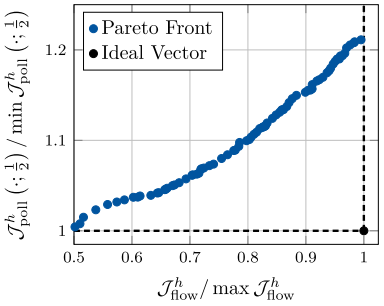

(a) Pareto front and ideal vector

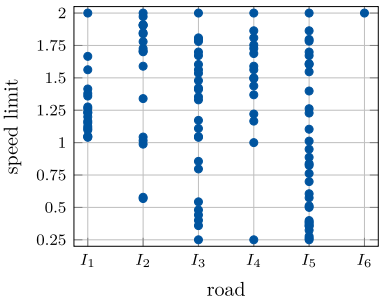

(b) Values of the Pareto-optimal speed limit policies

Fig. 10 The optimal solution of the proof-of-concept example with $\delta = 1/2$, i.e., air pollution is estimated by active traffic on the road network and idle traffic due to the queues

Next, we solve the proof-of-concept example with $\delta = 1/2$, i.e., the indicator measuring the environmental impact of vehicular traffic also accounts for idle traffic. Figure 10 visualizes the resulting optimal solution consisting of the Pareto front (Fig. 10a) and the Pareto-optimal speed limit policies (Fig. 10b). Again, the axes of the Pareto front are normalized by the optimal values of the objectives.

The Pareto front reveals that for this modeling approach maximizing the accumulated traffic flow results in an increase of the environmental impact by around 20% while minimizing the environmental impact decreases the flow by around 50% compared to its optimal value. An efficient point where neither of the objectives is ideal is, for example, the point $(0.8, 1.1)^\top$.

The Pareto-optimal speed limits policies are similar in terms of the range compared to the modeling approach where $\delta = 0$, i.e., they also indicate that the objectives are conflicting. However, we observe a subtle change in the range of the speed limits of the access road: The lowest set speed limit is $V_1^{\max} \approx 1$ compared to $V_1^{\max} = 0.25$ for $\delta = 0$. We can attribute this phenomenon to the idle traffic accounted by the indicator to measure air pollution caused by vehicular traffic. The indicator accounts for the idle traffic by adding the average accumulated queue length to $\mathcal{J}^h_{\text{diff}}$, which then creates an incentive to reduce the queue length. The correspondence between the queue length and the speed limits is the following: The supply of a road scales linearly with its speed limit, i.e., an increased speed limit results in a higher flow that can access the road. The more flow can access the road network, the less excess accrues, which results in a shorter queue.

We omit a discussion on specific speed limits policies if $\delta = 1/2$ as this would reveal the same issues that can be observed in Fig. 9b, where the modeling neglects the contribution of the idle traffic to air pollution.

At last, we compare the optimal solutions to the two modeling approaches (4.8) and (4.9). Therefore, we display the computed Pareto fronts in $(\mathcal{J}^h_{\text{flow}}, \mathcal{J}^h_{\text{poll}}(\cdot;\delta))$ coordinates for $\delta \in \{0, 1/2\}$, see Fig. 11, and in $(\mathcal{J}^h_{\text{diff}}, \mathcal{J}^h_{\text{queue}})$ coordinates, see Fig. 12. Notice, that we do not normalize the axis $\mathcal{J}^h_{\text{queue}}$ as the minimal value of $\mathcal{J}^h_{\text{queue}}$ is in fact zero.

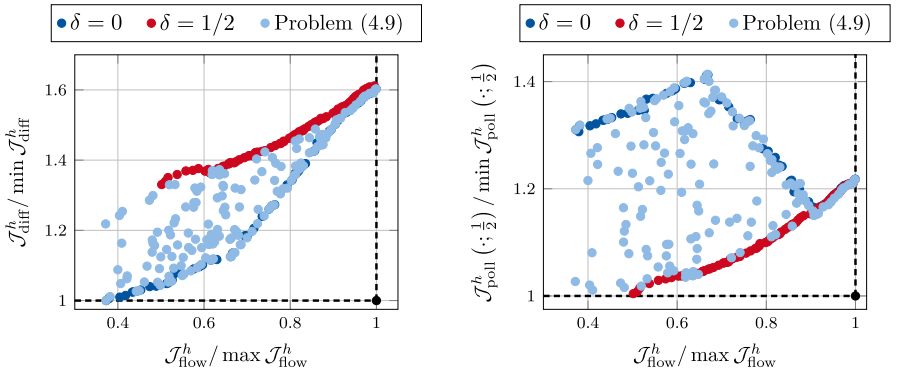

(a) $(\mathcal{J}^h_{\text{flow}}, \mathcal{J}^h_{\text{poll}}(\cdot;0))$ coordinates. (b) $(\mathcal{J}^h_{\text{flow}}, \mathcal{J}^h_{\text{poll}}(\cdot;1/2))$ coordinates.

Fig. 11 Comparison of the Pareto fronts of the optimization problem (4.8) for different values of δ, and of (4.9) by representing them in different coordinate systems. (color figure online)

Figure 11 shows that each Pareto front is Pareto-optimal in "its" coordinate system. If the accumulated traffic flow attains values close to its maximal value, the two fronts coincide for $\delta = 0$ and $\delta = 1/2$. Furthermore, we observe that the optimal solution to the optimization problem (4.9) involving three objectives, (a) lies between the two Pareto fronts involving only two, and (b) seems to have a tendency to share more efficient points with the solution to the problem (4.8) with $\delta = 0$. In Fig. 11a, we observe that the optimal solution corresponding to $\delta = 1/2$ allows a higher traffic flow in general and that the active traffic contributes more to air pollution compared to the optimal solution corresponding to $\delta = 0$. A possible cause may be the penalty for the presence of idle traffic in the case $\delta = 1/2$, which then allows "more" active traffic on the network in the attempt to reduce the contribution of idle traffic.

Further, in Fig. 11b, we see that the combined contribution of active and idle traffic to air pollution is higher in case $\delta = 0$ compared to the case $\delta = 1/2$. Again, a possible explanation may be that the indicator measuring the environmental impact also accounts for the idle traffic if $\delta = 1/2$, while the case $\delta = 0$ neglects it. Thus, to minimize the objective $\mathcal{J}^h_{\text{poll}}(\cdot; 1/2)$, the components corresponding to active and idle traffic both have to be reduced, while the minimization of $\mathcal{J}^h_{\text{poll}}(\cdot; 0)$ only requires a reduction of the contribution of active traffic.

Figure 12 plots the average mass of air pollutants in Ω against the average queue length and supports these findings. Among the three scenarios, the Pareto front to the problem (4.9) yields the lowest, individual contribution of active and idle traffic to air pollution. An explanation for this observation is that the optimization problem (4.9) tries to optimize three objectives: the traffic flow, the pollution caused by active, and the one caused by idle traffic. Hence, contribution of active and passive traffic to air pollution has to be as low as possible instead of its sum compared to problem (4.8) with $\delta = 1/2$. Furthermore, it becomes evident that $\delta = 1/2$ allows a higher traffic flow and shorter queues, while $\delta = 0$ allows a lower average mass of air pollutants in Ω. The reasoning is analogous to the discussion of the results presented in Fig. 11.

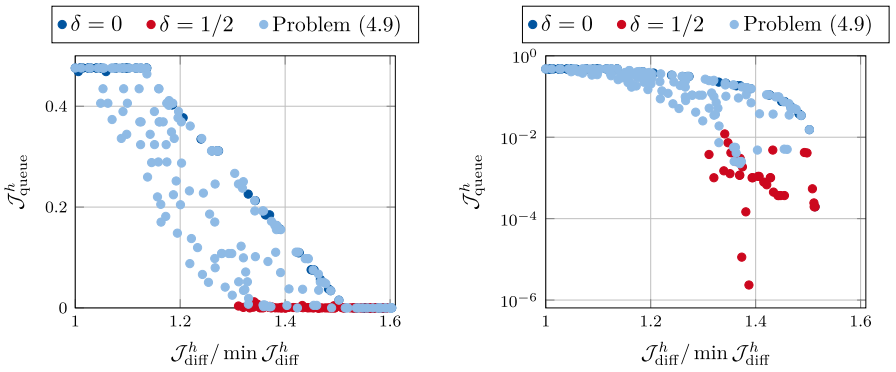

(a) Normal y-axis. (b) Logarithmic y-axis.

Fig. 12 Comparison of the contribution to air pollution caused by active traffic (measured by $\mathcal{J}^h_{\text{diff}}$) and idle traffic (measurement based on the average queue length). Both plots show the same image but the y-axis is scaled differently

7 Conclusions

We presented the framework of speed-limit dependent traffic emission models to simulate the air pollutant emission caused by vehicular and their spread given a fixed speed limit policy. Further, we used this framework together with the tool of multi-objective optimization to model our goal of achieving minimal air pollution while maximizing the traffic flow by adjusting the speed limit policy. The proof-of-concept example presented in Sect. 6 revealed that the two objectives of minimal air pollution and maximal traffic flow are conflicting, which means they are realized for different speed limit policies. The conflict between these objectives makes multi-objective optimization a valuable tool to determine optimal compromises in the sense of Pareto where neither of the objectives is optimal.

In future work, we aim to test the framework for more complex and realistic scenarios, possibly incorporating a second-order traffic model as presented in Balzotti et al. (2022) because these models allow to estimate the emissions based on the vehicles' speed and acceleration.

Acknowledgements S.G. thanks the Deutsche Forschungsgemeinschaft (DFG, German Research Foundation) for the financial support through GO1920/11-1 and 12-1 within the SPP 2410 Hyperbolic Balance Laws in Fluid Mechanics: Complexity, Scales, Randomness (CoScaRa). M.H. thanks the Deutsche Forschungsgemeinschaft (DFG, German Research Foundation) for the financial support under Germany's Excellence Strategy EXC-2023 Internet of Production 390621612 and under the Excellence Strategy of the Federal Government and the Länder, 333849990/GRK2379 (IRTG Hierarchical and Hybrid Approaches in Modern Inverse Problems), 320021702/GRK2326, 442047500/SFB1481 within the projects B04, B05 and B06, through SPP 2410 Hyperbolic Balance Laws in Fluid Mechanics: Complexity, Scales, Randomness (CoScaRa) within the Project(s) HE5386/26-1 and HE5386/27-1, and through SPP 2298 Theoretical Foundations of Deep Learning within the Project(s) HE5386/23-1, Meanfield Theorie zur Analysis von Deep Learning Methoden (462234017). Support through the EU DATAHYKING No. 101072546 is also acknowledged.

Author Contributions S.G. and A.U. worked on the problem description and numerical simulation while M.H. provided the theoretical foundation and test instances. All authors reviewed the manuscript.

Funding Open Access funding enabled and organized by Projekt DEAL.

Declarations

Conflict of interest The authors declare that they have no conflict of interest.

References

Aljanahi A, Rhodes A, Metcalfe A (1999) Speed, speed limits and road traffic accidents under free flow conditions. Accid Anal Prev 31:161–168. https://doi.org/10.1016/S0001-4575(98)00058-X

Alvarez-Vázquez L, García-Chan N, Martínez A, Vázquez-Méndez M (2008) Pareto-optimal solutions for a wastewater treatment problem. J Comput Appl Math 234(7):2193–2201. https://doi.org/10.1016/j.cam.2009.08.076

Alvarez-Vázquez L, García-Chan N, Martínez A, Vázquez-Méndez M (2010) Multi-objective Pareto-optimal control: an application to wastewater management. Comput Optim Appl 46:135–157. https://doi.org/10.1007/s10589-008-9190-9

Alvarez-Vázquez LJ, García-Chan N, Martínez A, Vázquez-Méndez ME (2015) An application of interactive multi-criteria optimization to air pollution control. Optimization 64:1367–1380. https://doi.org/10.1080/02331934.2014.951044

Alvarez-Vázquez LJ, García-Chan N, Martínez A, Vázquez-Méndez ME (2017) Numerical simulation of air pollution due to traffic flow in urban networks. J Comput Appl Math 326:44–61. https://doi.org/10.1016/j.cam.2017.05.017

Alvarez-Vázquez LJ, García-Chan N, Martínez A, Vázquez-Méndez ME (2018) Optimal control of urban air pollution related to traffic flow in road networks. Math Control Relat Fields 8(1):177–193. https://doi.org/10.3934/mcrf.2018008

Balzotti C, Briani M, De Filippo B, Piccoli B (2022) A computational modular approach to evaluate NO_x emissions and ozone production due to vehicular. Discrete Contin Dyn Syst B 27(6):3455–3486. https://doi.org/10.3934/dcdsb.2021192

Berrone S, De Santi F, Pieraccini S, Marro M (2012) Coupling traffic models on networks and urban dispersion models for simulating sustainable mobility strategies. Comput Math Appl 64(6):1975–1991

Branke J, Kalyanmoy D, Miettinen K, Slowinski R (2008) Mulitobjective optimization. Springer, Berlin

Brink M, Mathieu S, Rüttener S (2022) Lowering urban speed limits to 30 km/h reduces noise annoyance and shifts exposure-response relationships: evidence from a field study in Zurich. Environ Int. https://doi.org/10.1016/j.envint.2022.107651

Cascone A, D'Apice C, Benedetto P, Luigi R (2007) Optimization of traffic on road networks. Math Models Methods Appl Sci 17(10):1587–1617

Coclite GM, Garavello M, Piccoli B (2005) Traffic flow on a road network. SIAM J Math Anal 36(6):1862–1886. https://doi.org/10.1137/S0036141004402683

D'Amato G, Cecchi L (2008) Effects of climate change on environmental factors in respiratory allergic diseases. Clin Exp Allergy 38:1264–1274. https://doi.org/10.1111/j.1365-2222.2008.03033.x

Ehrgott M (2005) Multicriteria optimization. Springer, Berlin. https://doi.org/10.1007/3-540-27659-9

Epstein P (2005) Climate change and human health. N Engl J Med 353(14):1433–1436. https://doi.org/10.1056/NEJMp058079

Garavello M, Piccoli B (2006) Traffic flow on networks. American Institute of Mathematical Sciences, Springfield
Garavello M, Han K, Piccoli B (2016) Models for vehicular traffic on networks. Am Inst Math Sci. https://doi.org/10.1007/978-3-642-22261-0
García-Chan N, Alvarez-Vázquez LJ, Martínez A, Vázquez-Méndez ME (2022) Bilevel optimal control of urban traffic-related air pollution by means of Stackelberg strategies. Optim Eng 23:1165–1188. https://doi.org/10.1007/s11081-021-09636-w
Goatin P, Göttlich S, Kolb O (2016) Speed limit and ramp meter control for traffic flow networks. Eng Optim 48(7):1121–1144. https://doi.org/10.1080/0305215X.2015.1097099
Göttlich S, Herty M, Ziegler U (2015) Modeling and optimizing traffic light settings in road networks. Comput Oper Res 55:36–51. https://doi.org/10.1016/j.cor.2014.10.001
Greenshields BD, Bibbins JR, Channing WS, Miller HH (1935) A study of traffic capacity. In: Highway research board proceedings. National Research Council (USA), Highway Research Board
Herty M, Lebacque J-P, Moutari S (2009) A novel model for intersections of vehicular traffic flow. Netw Heterog Media 4:813–826
Int Panis L, Broekx S, Liu R (2006) Modelling instantaneous traffic emission and the influence of traffic speed limits. Sci Total Environ 371:270–285. https://doi.org/10.1016/j.scitotenv.2006.08.017
LeVeque RJ (1992) Numerical methods for conservation laws. Birkenhäuser-Verlag
Lighthill MJ, Whitham G (1955) On kinematic waves. II. A theory of traffic flow on long crowded roads. Proc R Soc Lond Ser A Math Phys Sci 229(1178):317–345
MATLAB and Optimization Toolbox Release (2022) The MathWorks Inc. Natick, p 2022
Parra-Guevara D, Skiba YN (2003) Elements of the mathematical modeling in the control of pollutants emissions. Ecol Model 167:263–275. https://doi.org/10.1016/S0304-3800(03)00191-1
Pasquier M, Jay S, Jacob J, Sagaut P (2023) A Lattice–Boltzmann-based modeling chain for traffic-related atmospheric pollutant dispersion at the local urban scale. Build Environ 6:66
Ramanatha V, Feng Y (2009) Air pollution, greenhouse gases and climate change: global and regional perspectives. Atmos Environ 43:37–50. https://doi.org/10.1016/j.atmosenv.2008.09.063
Richards PI (1956) Shock waves on the highway. Oper Res 4(1):42–51
Skiba YN, Parra-Guevara D (2000) Industrial pollution transport. Part 1. Formulation of the problem and air pollution estimates. Environ Model Assess 5:169–175. https://doi.org/10.1023/A:1019065728972
Stockie JM (2011) The mathematics of atmospheric dispersion modeling. SIAM Rev 53(2):349–372. https://doi.org/10.1137/10080991X
Treiber M, Kesting A (2013) Traffic flow dynamics: data, models, and simulation. Springer, Berlin. https://doi.org/10.1007/978-3-642-32460-4
Vázquez-Méndez ME, Alvarez-Vázquez LJ, García-Chan N, Martínez A (2019) Optimal management of an urban road network with an environmental perspective. Comput Math Appl 77:1786–1797. https://doi.org/10.1016/j.camwa.2018.06.021
Wesseling P (1996) von Neumann stability conditions for the convection–diffusion equation. IMA J Numer Anal 16(4):583–598. https://doi.org/10.1093/imanum/16.4.583
Zegeye SK, De Schutter B, Hellendoorn J, Breunesse EA (2011) Variable speed limits for green mobility. In: 2011 14th International IEEE conference on intelligent transportation systems (ITSC). IEEE, pp 2174–2179. https://doi.org/10.1109/ITSC.2011.6082833